Evaluation of Jet Mixing Rate Based on DNS Data of Excitation Jets

Tsujimoto, K. Kariya, S., Shakouchi, T. and Ando, T.
Division of Mechanical Engineering, Graduate School of Engineering, Mie University,
1577 Kurimamachiya-cho, Tsu, 514-8507 Japan
tujimoto@mach.mie-u.ac.jp

Abstract
In order to establish a good measure of mixing rate, jet mixing is examined using the DNS (direct numerical simulation) data of controlled jets. In the computation, spatial discretization is performed using a hybrid scheme that adopts a sixth-order compact scheme in the streamwise direction and a Fourier series in the lateral directions. The Reynolds number is 1500. Two measures such as statistical entropy and a mixedness parameter are investigated using a passive scalar concentration. Compared with simple measures, i.e., jet width, centerline velocity, and turbulent kinetic energy, it is found that the statistical entropy is a good measure for representing the mixing state in different controlled jets, and it is possible to use the fluctuating entropy to detect a highly mixed region and determine the correlation of the mixed regions with the vortical structure. In addition to statistical entropy, the mixedness parameter is also found to have useful properties for the estimation of mixing efficiency. These findings suggest that these measures are expected to contribute to the optimization of jet mixing.

Key Words: Active control, DNS, Jet, Mixing, Coherent structure

1. INTRODUCTION
In order to enhance mixing or diffusion in many industrial applications, jet mixing control has been examined. The control methods used for jet mixing are categorized into either passive or active methods. Irrespective of the method, understanding the mixing state is indispensable for realizing an effective jet control. The results of liner stability analyses reveal that there are two types of dominant modes characterizing the large-scale flow structures near field of a jet, namely, varicose and helical modes, and diffusion or mixing is effectively controlled through these modes. Further, it is well known that a complex jet is made of a combination of these modes (Reynolds [1]). For example, a flapping mode comprises a pair of helical modes with the same frequency and the same amplitude. Further, it is experimentally confirmed that when the axial mode is added to them, a bifurcating jet or a blooming jet is formed (Reynolds [1]). Such an active control was also investigated using DNS (direct numerical simulation) (Hilgers [2], Silva [3]), and induced the generation of strong diffusion. Although the effectiveness of these active control methods has already been demonstrated thus far, using simple estimations involving the jet width, mean streamwise velocity, turbulence intensity, and so on, it is not well enough to estimate the mixing efficiency using the reliable procedure. On the other hand, we investigated compound jets (Tsujimoto [4]) and found that their mixing efficiency could not be determined using the simple measure developed for an axisymmetric jet. Therefore, it is important to determine an appropriate measure for quantifying the mixing efficiency.

In the present study, we compared the validity and usefulness of the new measures, i.e., statistical entropy (Everson [5], Chikahisa [6]) and the mixedness parameter (Cetegen et al. [7], Tseng [8]), with those of the conventional measures.

2.NUMERICAL METHOD
2.1 Governing equation and discretization
Under the assumption of incompressible and isothermal flow, the dimensionless governing equations are as follows:

$$\frac{\partial u_i}{\partial x_i} = 0 \tag{1}$$

$$\frac{\partial u_i}{\partial t} + h_i = -\frac{1}{\rho}\frac{\partial p}{\partial x_i} + \frac{1}{\mathrm{Re}}\frac{\partial^2 u_i}{\partial x_j \partial x_j} \tag{2}$$

$$(h_i = \varepsilon_{ijk}\omega_j u_k,\ \ \omega_j : vorticity)$$

$$\frac{\partial T}{\partial t} + \frac{\partial u_i T}{\partial x_i} = \frac{1}{\mathrm{RePr}}\frac{\partial^2 T}{\partial x_i \partial x_i} \tag{3}$$

The nonlinear terms are expressed in the rotational form $\boldsymbol{\omega} \times \boldsymbol{u}$ to conserve the total energy; therefore, p represents the total pressure. For the characteristic length and velocity, the nozzle diameter D and the streamwise velocity $V_0 = V_1 - (V_1, V_2$ refer to Eq. (6)) were chosen for nondimensionalization, respectively. The Reynolds number is defined as Re $V_0 = D/\nu$ (ν: kinematic viscosity). A Cartesian coordinate system is employed in which y is the streamwise direction and x and z are the lateral directions.

Spatial discretization is performed using a hybrid scheme that adopts a sixth-order compact scheme (Lele [9]) in the streamwise direction and a Fourier series in the lateral directions. In order to remove the numerical instability due to the nonlinear terms, the 2/3-rule is applied to the lateral directions, and implicit filtering is carried out for the streamwise direction using the sixth-order compact scheme. A third-order Adams-Bashforth method is used for time advancement. The well-known MAC scheme [10] is employed for pressure-velocity coupling, which generates a Poisson equation for the pressure. After the Poisson equation is Fourier transformed in the x and z directions, independent differential equations are obtained for each wave number and then discretized using the sixth-order compact scheme. Finally, a pentadiagonal matrix is deduced for each wave number. In the present simulation code, the matrix is solved using the LU decomposition method. The outerflow boundary condition is introduced for both the momentum and the energy equations by solving the following simplified convective equations:

$$\frac{\partial u_i}{\partial t} + u_c \frac{\partial u_i}{\partial y} = 0 \tag{4}$$

$$\frac{\partial T}{\partial t} + u_c \frac{\partial T}{\partial y} = 0 \tag{5}$$

In the present simulations, the convective velocity is set to $u_c = 0.5V_0$.

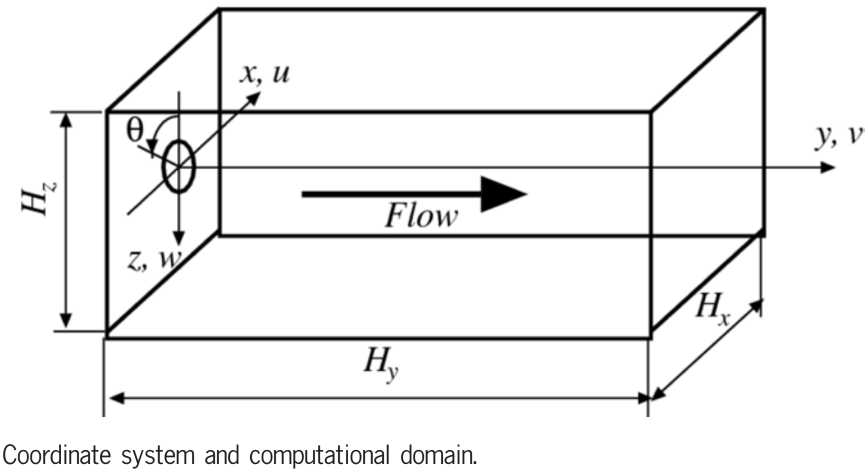

Figure 1. Coordinate system and computational domain.

2.2 Calculation conditions

As an inflow condition, the inflow mean velocity distribution is determined by referring to the literature (Silva [3]).

$$V_b(r) = \frac{V_1 + V_2}{2} - \frac{V_1 - V_2}{2}\tanh\left[\frac{1}{4}\frac{R}{\theta_0}\left(\frac{r}{R} - \frac{R}{r}\right)\right], \tag{6}$$

where V_1 is the jet centerline velocity, and V_2 is a co-flow velocity. $R(= D/2)$ is the jet radius, and θ_0 is the momentum thickness of the initial shear layer. r denotes the radial distance from the jet centerline. In the present simulations, the jet velocities and initial momentum thickness are set to $V_1 = 1.075V_0$, $V_2 = 0.075V_0$, and $R/\theta_0 = 20$, respectively. The inflow temperature is prescribed by the same inlet velocity distribution, V_b. The size of the computational domain is set to $H_x \times H_y \times H_z = 7D{\times}15D{\times}7D$, except for the flapping excitation case ($H_x = H_y = 10D$ for the flapping case). The grid $N_x \times N_y \times N_z$ is $256 \times 200 \times 256$. The Reynolds number Re is equal to 1500, and the Prandtl number Pr is equal to 0.707. For low-speed flow, there is a small quantity of experimental data, enabling a comparison of the present results. As shown in a previous paper [4], we confirmed that the data for a free jet is in good agreement with the experimental data for the centerline velocity and turbulent kinetic energy.

2.3 Excitation types

In order to enhance mixing using active control, three types of excitations are considered: axial (V_a), helical (V_h), and flapping (V_f) excitations. In each type of excitation, a random perturbation with 1% of the strength of V_0, V_{rand} (x, z, t), along with the following perturbation velocity are superposed on the inflow mean velocity V_b. The inflow velocity V_{in} is expressed as follows for each excitation:

$$V_{in}(x,z,t) = V_b(r) + V_{rand}(x,z,t) + \begin{Bmatrix} V_a \\ V_h \\ V_f \end{Bmatrix} \tag{7}$$

where

$V_a = \varepsilon_a \sin(2\pi\, \mathrm{St_a}\, t^*)V_b$,
$V_h = \varepsilon_h \sin(\theta - 2\pi\, \mathrm{St_h}\, t^*)V_b$, and
$V_f = \varepsilon_f[\sin(\theta - 2\pi\, \mathrm{St_h}\, t^*) - \sin(\theta + 2\pi\, \mathrm{St_f}\, t^*)]V_b$,

t^* represents a nondimensionalized time, $t^* = tV_0/D$, and $\varepsilon_{a,h,f}$, is the strength of the excitation. θ is the azimuthal angle shown in Fig. 1. The Strouhal number $St_{a,h,f}$ is defined as $St = fD/V_0$ (where f is the frequency). It is well known that a peculiar instability mode is induced in the near field of a jet, according to the excitation. In the case of axial excitation, a column of vortex rings is formed upstream, and in the case of helical excitation, helical-like vortical structures appear. In the case of flapping excitation, the flow structures are distorted in one radial direction, and strong anisotropic mixing occurs downstream.

The frequency of the instability mode associated with the generation of large-scale structures induced by column instability near the end of the potential core of the jet is the so-called "preferred mode."

Since the preferred mode is influenced by the shape of the nozzle or the boundary layer thickness near the nozzle exit, the preferred mode St_p becomes $0.25 < St_p < 0.5$ (Hussain et al.[11]). In the present simulation, the excitation frequency is set to $St_a = St_h = St_f = 0.4$, and the strength of the excitation is set to $\varepsilon_a = \varepsilon_h = \varepsilon_f = 0.05$.

2.4 Mixing measures based on the passive scalar concentration

2.4.1 Statistical entropy

In order to quantify the mixing state, Everson et al. [5] investigated the statistical entropy based on the passive scalar concentration, and they demonstrated the characteristics of this measure by examining the experimental data.

In the following, we provide a simple explanation of this measure.

Boltzmann proposed the statistical entropy, which is defined as the logarithm of combination, W.

$$S = k \ln W , \tag{8}$$

where k is the Boltzmann constant. W is the combination of the number of molecules in the i-th coarse-grained cell, N_i.

$$W = \frac{N!}{N_1! N_2! \cdots N_M!} = \frac{N!}{\Pi N_i!} \tag{9}$$

where N is the total number of molecules. If N is sufficiently large, Stirling' s approximation, $\ln L! \approx L \ln L - L$, can be applied to Eq. (8) as follows:

$$S = k\left[N \ln N - \sum_{i=1}^{M} N_i \ln N_i \right]. \tag{10}$$

If the space is divided to M cells, and all the molecules exist in a single cell, $S = 0$. However, if the molecules are uniformly distributed to each cell, i.e., $N_i = N/M$, the maximum entropy $S = kN \ln M$. Since incompressible flow is assumed in the present study, the temperature can be related to the concentration of the passive scalar, i.e., $\phi = (T - T_2)/(T_1 - T_2)$.

Considering the small volume surrounding a grid point i, ΔV (= $\Delta_x \Delta_y \Delta_z$), the number of molecules is denoted by $N_i = \phi_i \Delta V$; therefore,

$$S = k\Delta V\left[\Phi \ln \Phi - \sum_{i=1}^{M} \phi_i \ln \phi_i \right], \tag{11}$$

where $\Phi = \sum \phi_i$.

2.4.2 Mixedness parameter

Cetegen and Mohamad [7] proposed the use of mixedness Mp as a mixing measure. Tseng et al. [8] estimated the mixing of coastal flow using this parameter.

The mixedness parameter is defined as follows:

$$Mp = \frac{1}{V} \int_V \phi(1-\phi) dV, \tag{12}$$

where V is the total volume of the considered domain.

If bimolecular mixing is considered, ϕ represents the concentration of one type of molecule, and $1 - \phi$ represents that of another type of molecule. Therefore, for a completely unmixed state ($\phi = 0$ and $= 1$), $Mp = 0$, and for a fully mixed state ($\phi = 0.5$), $Mp = 0.25$. Compared to statistical entropy, it can be seen that Mp is intuitively derived.

3. RESULTS

3.1 Structure of controlled jets

In order to visualize the vortical structure, the iso-surfaces of the second invariance of velocity gradient tensor at Q ($= -\partial u_i/\partial x_j \cdot \partial u_j/\partial x_i$) = 0.2 are shown in Fig. 2. In each figure, the image on the left is the side view, while that on the right is the view looking directly at the nozzle.

In Fig. 2(a), due to a Kelvin-Helmholtz instability occurring upstream, quasi-periodically vortex-ring-like structures are generated. As the vortex rings breakdown downstream, tube-like vortical structures are formed. In the case of axial excitation (Fig. 2(b)), depending on the excitation frequency, strong vortical structures are regularly formed and retained for a while from upstream to downstream. As shown in this figure, the vortex rings do not successively interact with each other. However, when a vortex ring rapidly breaks down, the formation of quasi-streamwise vortices is observed downstream. In the case of helical excitation (Fig. 2(c)), helical-like structures are continuously formed from upstream to downstream. The breakdown in this case occurs earlier than in the abovementioned cases

(a) Normal

(b) Axial excitation

(c) Helical excitation

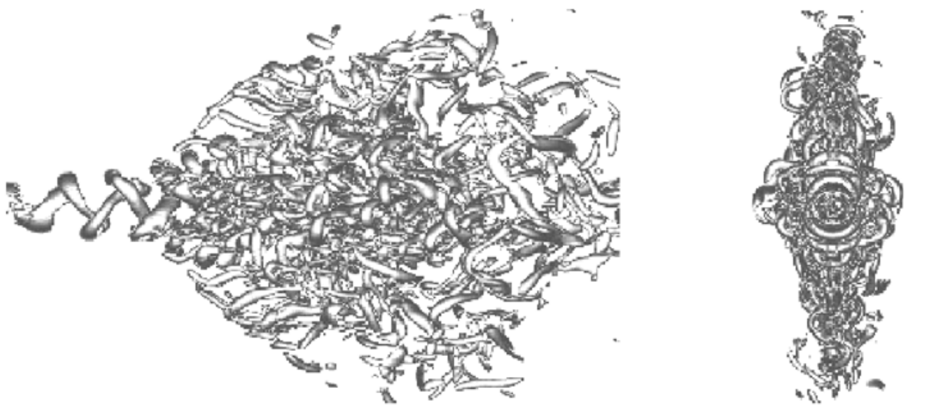

(d) Flapping excitation

Figure 2. Instantaneous vortex structure visualized at Q = 0.2

because the streamwise vorticity component is included at an earlier stage of evolution. In the case of flapping excitation (Fig. 2(d)), the jet markedly diffuses for one direction. This is because after issuing from the nozzle, strong hair-pin-like structures are alternately formed upstream. The visualized flow structures of all these cases are in agreement with the previous DNS (Silva [3], Urban [12]). Therefore, the present results are confirmed to be correct under the giving excitation conditions.

3.2 Simple measure for jet mixing

As a measure of mixing rate, various flow properties such as the centerline velocity, jet width, and turbulence intensity have been considered.

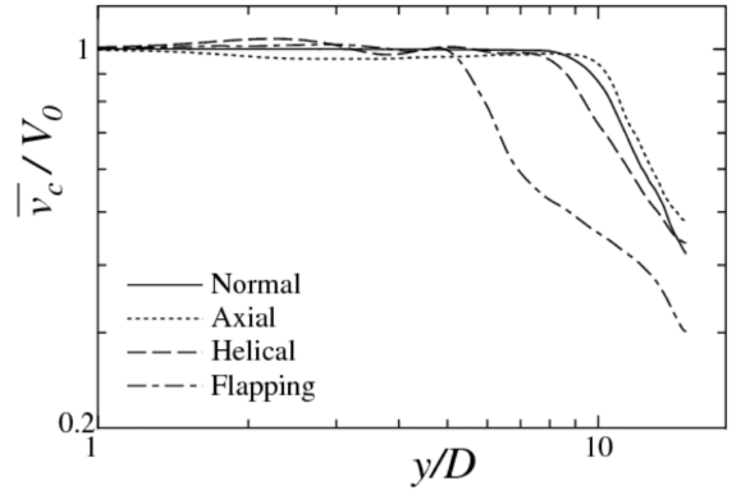

Figure 3. Distribution of mean centerline velocity

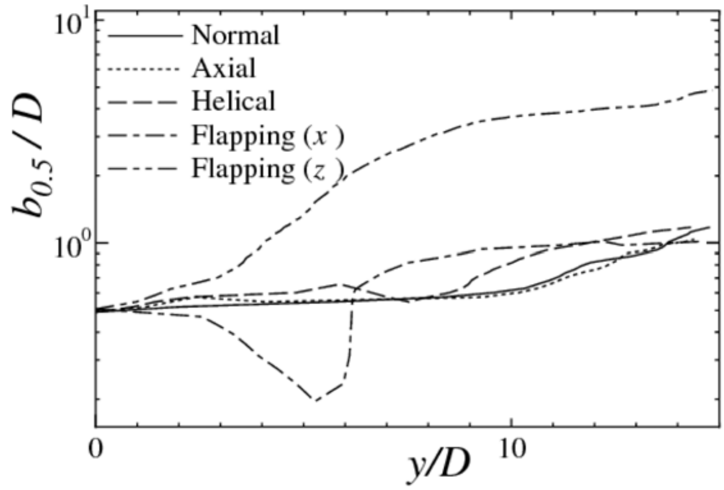

Figure 4. Distribution of half jet width.

Figure 3 shows the distribution of the centerline velocity $\overline{v}_c = \overline{v}(0, y, 0)$. Corresponding to the visualized coherent structures, the breakdown position of the potential core in the flapping case, $y/D \approx 5$, is located more upstream than in the other cases. Except for the flapping case, the breakdown position is shifted downstream in the order of the helical, normal, and axial excitations. In particular, contrary to our intuition, the decay of the centerline velocity in the axial excitation case is shifted downstream as compared to the normal case. As might be expected, the starting position of the velocity decay is largely delayed as compared to the visualized structure.

The jet half width $b_{0.5}$ is shown in Fig. 4. In the normal and axial excitation cases, the jet expands at the same rate from the downstream position (y/D = 10) at which the ring-like vortex structures begin to break down. While in the helical excitation case, although the half width behaves singularly near y/d = 5, at which vortex breakdown occurs, roughly speaking, the jet expands widely compared to both the normal and axial cases. In the flapping case, the jet markedly expands in one direction (z), and shrinks in another direction (x), demonstrating an anisotropic distribution. Although it is not shown here, the shrinkage of the jet width in the x direction was confirmed from the iso-contour of the mean streamwise velocity. Compared to the centerline velocity distribution, the jet width makes it possible to capture the diffusion rate. However, if the anisotropic pattern of jet diffusion occurs, or if jets are combined, it is difficult to uniquely define the jet width, suggesting that estimation using the jet width is limited to a simple jet.

Figure 5 shows the distribution of the turbulent kinetic energy (TKE), $k(= 0.5u'^2_{i,rms})$. Figure 5(a) shows the centerline distribution of TKE, $k_c = k(0, y, 0)$. In all the excitation cases, turbulence near $y/D \approx 5$ is strongly generated by the coherent structure induced by the excitation. Corresponding to the visualized structures, in the normal, axial, and helical excitation cases, turbulence generation is rapidly promoted downstream as the breakdown of the vortical structures proceeds. However, in the flapping case, since the vortex breakdown considerably proceeds as compared to the other cases, the secondary peak downstream does not appear.

Figure 5(b) shows the distribution of the integrated turbulent kinetic energy defined by Eq. (13).

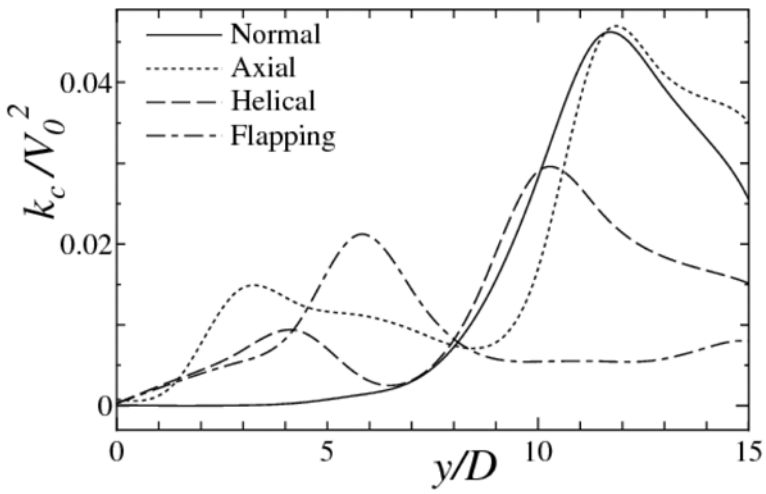

(a)

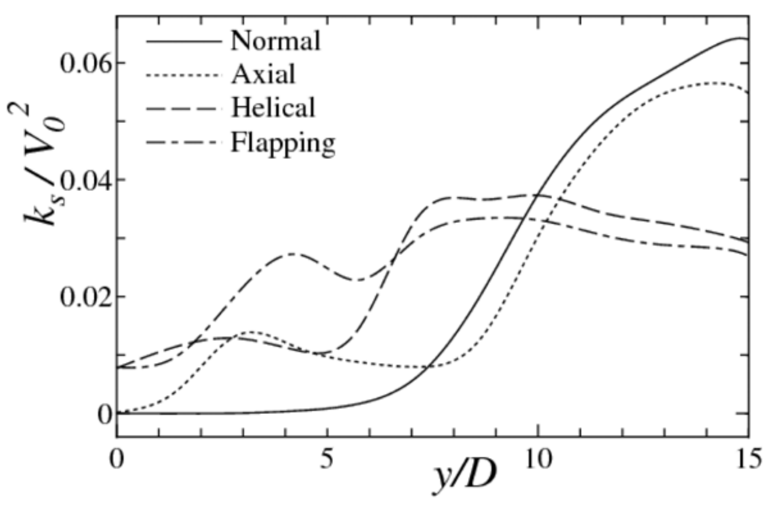

(b)

Figure 5. Distribution of turbulence kinetic energy, (a) centerline value and (b) integrated value from Eq. (13).

$$k_s = \int_{-H_x/2}^{H_x/2} \int_{-H_{z/2}}^{H_z/2} 0.5k \mathrm{d}x \mathrm{d}z \tag{13}$$

Considering the mixing state, the flapping case should be the most enhanced. However, the amounts of turbulent kinetic energy in the helical and flapping cases are obviously less than in the normal and axial cases. In general, the generation of turbulent kinetic energy is determined by the product of the mean shear and the Reynolds stresses.

Since the mean shear is weakened more if the breakdown is more promoted, the amount of turbulence does not always increase.

These findings suggest that the turbulence intensity provides information about the position where the mixing is enhanced, but cannot be used as a qualitative measure for the mixing rate.

3.3 Evaluating the mixing measure based on the passive scalar concentration

We next evaluate the abovementioned measures, i.e., the statistical entropy and the mixedness parameter.

In order to investigate the streamwise variation of the statistical entropy, S is summed over the plane perpendicular to the streamwise direction, and $\overline{S}$ is defined as S normalized with the inflow quantity, S_0. M represents the number of grids on the x-z plane; $M = 65{,}536$ ($= 256 \times 256$).

As shown in Fig. 6(a), the statistical entropy increases downstream in the order of the axial, helical, and flapping cases. This is reflected in the increase of randomness downstream and the mixing enhancement due to the excitations. In particular, in the axial excitation, the entropy increases until $y/D = 2$, and then becomes nearly constant until $y/D = 10$. This is because the vortical structures move downstream without the breakdown, which suggests that the aggressive formation of a vortex ring does not always contribute to the promotion of jet mixing.

Here it should be noted that the first term on the *r.h.s* in Eq. (10) expresses the total number of molecules, N, and is two orders of magnitude larger than the second term on the *r.h.s*. When a larger total number of molecules exists, the statistical entropy is greater. In other words, this measure reflects the physical property corresponding to the jet expansion. However, if the same number of molecules is distributed between different jets, the first terms of Eq. (10) does not represent the difference concerning the mixing property; thus it seems that the second term of Eq. (10) includes the substantial properties for mixing, despite the fact that the magnitude of this term is smaller than that of the first one. The second term is defined as fluctuating entropy, S':

$$S' = -\sum_{i=1}^{M} \phi_i \ln \phi_i \ . \tag{14}$$

As shown in Fig. 6(a), $\overline{S}'$ is defined as the quantity S' normalized with the inlet value. As shown in Fig. 6, $\overline{S}'$ and $\overline{S}$ are not quantitatively, but qualitatively, similar.

Figure 7 shows the distribution of the mixedness parameter, which is defined by integrating the component, $\phi(1-\phi)$ on the cross sectional x-z plane. Although there is a quantitative difference between the two measures, it is found that the trend of the mixedness parameter behaves in a manner similar to that of the statistical entropy. Despite the fact that the derivations of the two measures are distinct, both parameters make it possible to quantify the efficiency of the jet mixing.

3.4 Relationship between the mixing measure and the flow structure

In order to determine the location of the highly mixed region, the mixing measures are observed. Figures 8(a)–(d) show the iso-contours of the component of fluctuating entropy, $-\phi \ln \phi$, on the y–z plane through the jet centerline. Figure 8(e) shows the iso-contour of the mixedness parameter. In all cases, it is found that the component of fluctuating entropy becomes strong in the region where the strong shear near the inlet exists and where the vortical structures are generated, and further downstream mixing measure distributes according to the jet expansion. In addition, Figure 8(e) also confirms that the mixedness parameter has a trend that is similar to statistical entropy.

It is clarified that except for the flapping case, the mixed region does not extend near the jet axis. Although it is found that the turbulence near the jet axis becomes strong at an early stage of flow development from Fig.5, however, the mixed region occurs only in the region where the entrainment

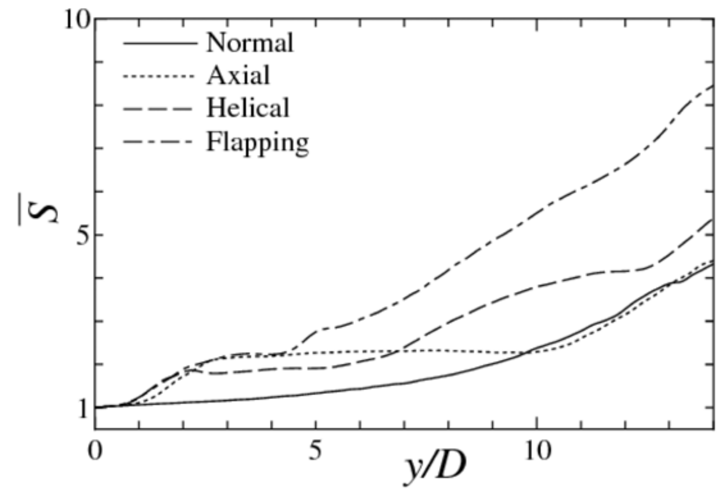

(a)

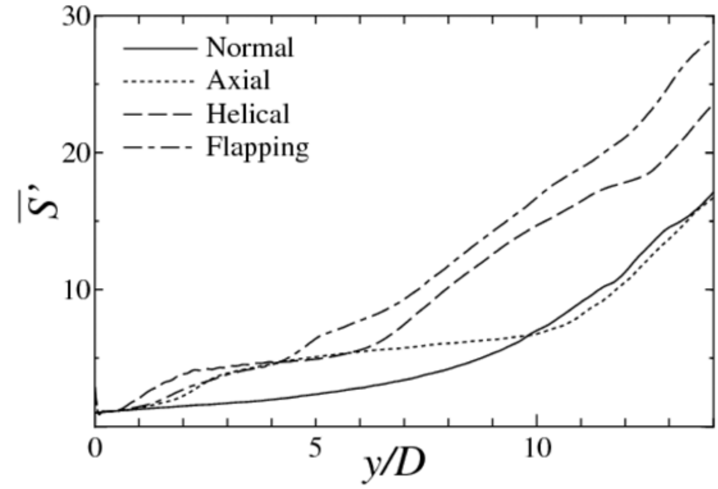

(b)

Figure 6. Distributions of (a) total entropy and (b) fluctuating entropy

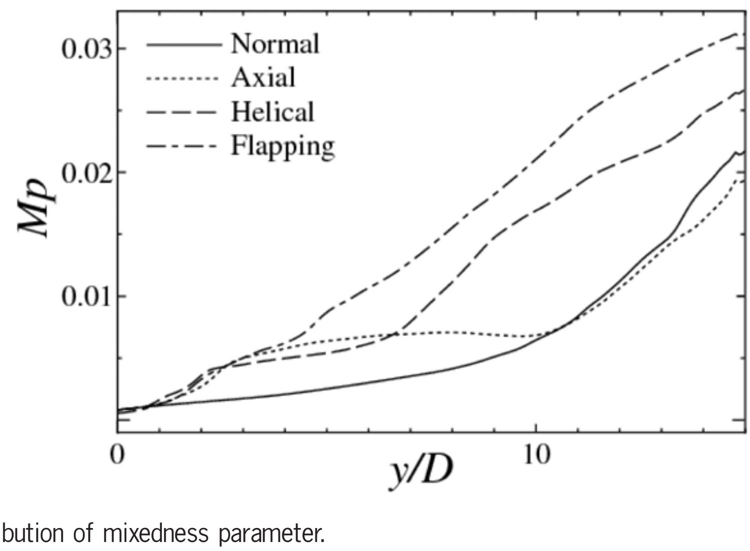

Figure 7. Distribution of mixedness parameter.

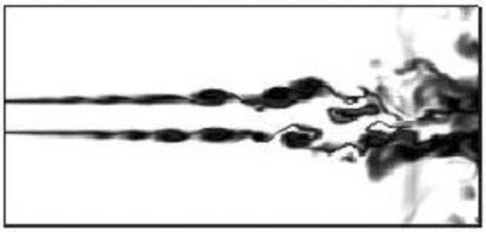

(a) Normal

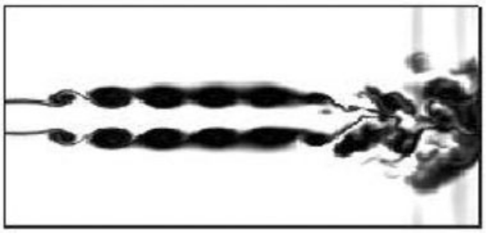

(b) Axial excitation

(c) Helical excitation

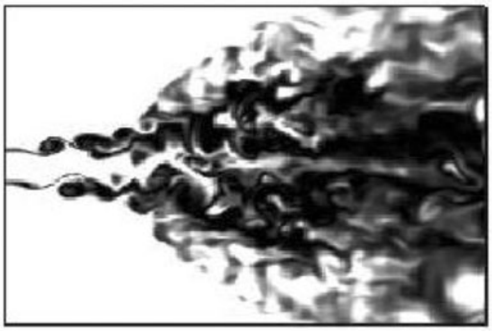

(d) Flapping excitation

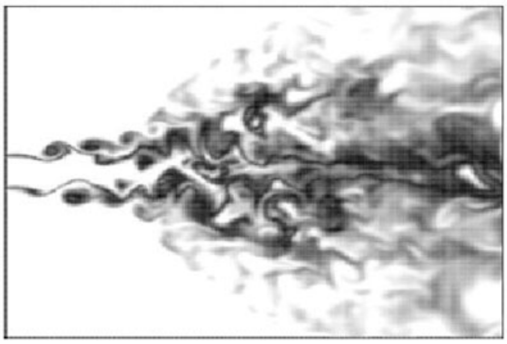

(e) Flapping excitation

Figure 8. Contour of component of mixing measure on x–y plane, (a)–(d) for the statistical entropy, (e) for the mixedness parameter.

of the surroundings is active. Due to entrainment, further downstream the mixed region extends even near the jet axis, and the flow becomes more chaotic.

Since these measures are convected to downstream, mixed region is affected by the upstream history and the upstream effect is accumulated downstream. Therefore, in order to investigate where the greatest mixing process occurs, we can consider the production rate of a mixing measure based on its transport equations. Converting the temperature to the scalar concentration, the transport equations of mixing measure are derived as follows:

For statistical entropy:

$$\frac{\mathrm{D}(-\phi\ln\phi)}{\mathrm{D}t} = \frac{1}{\mathrm{Re\,Pr}}\left[\nabla^2(-\phi\ln\phi) + \frac{(\nabla\phi)^2}{\phi}\right] \tag{15}$$

Similarly, for the mixedness parameter:

$$\frac{\mathrm{D}\phi(1-\phi)}{\mathrm{D}t} = \frac{1}{\mathrm{Re\,Pr}}\left[\nabla^2\phi(1-\phi) + 2(\nabla\phi)^2\right]. \tag{16}$$

In both the equations, the first term on the r.h.s. expresses the diffusion and does not contribute to a substantial change in the mixing measure. The second terms in both the equations always have positive values, they represent the substantial production term of the mixing measure.

Note that the second terms express scalar dissipation, and the generation of mixing is related to the region where the gradient of the scalar becomes strong.

Figures 9(a)–(d) show the iso-contours of the second terms on the *r.h.s.* of Eq. (15), $2(\nabla\phi)^2/(\mathrm{Re\ Pr}\ \phi)$. Figure 9(e) shows that of the mixedness parameter. The upstream high value of this term distributes in relation to the high shear around the vortical structures, in particular, the higher value seems to be related to the region where the stretching between vortical structures is enhanced. Further downstream, the distribution seems to be chaotic, similar to Fig. 8. The enhanced production region is located locally near the beginning of the vortex breakdown. Moreover, that of the mixedness parameter behaves in a manner similar to that of statistical entropy.

Since the gradient of the scalar should become strong to enhance the molecular diffusion, Figures 9 show that the stretching should be enhanced in order to activate mixing.

These measures are in accordance with the well-known physical properties of jet mixing. At the same time, it is expected that the local mixing state is comprehended, allowing the establishment of a control method.

CONCLUSIONS

We investigated a measure for jet mixing based on the passive scalar concentration using the DNS database of controlled jets. This led to the following conclusions:

1. A simple measure for the mixing state, such as the centerline velocity, jet width, or turbulence intensity, can be used as a rough index. In addition, since these measures are constructed based on an axisymmetric jet, they are not useful for comparing the mixing efficiency of a complex jet such as a flapping case.
2. In order to determine mixing measures based on the passive scalar concentration, the statistical entropy and the mixedness parameter were investigated. From the results of this investigation, it was shown that these measures have similar abilities to correctly evaluate the mixing efficiencies of different jets.
3. From instantaneous views of the components of these mixing measures, these quantities and the production terms of their transport equations were also found to be strongly correlated to the vortical structures, suggesting that the components of these new measures enable the detection of the local mixed state.

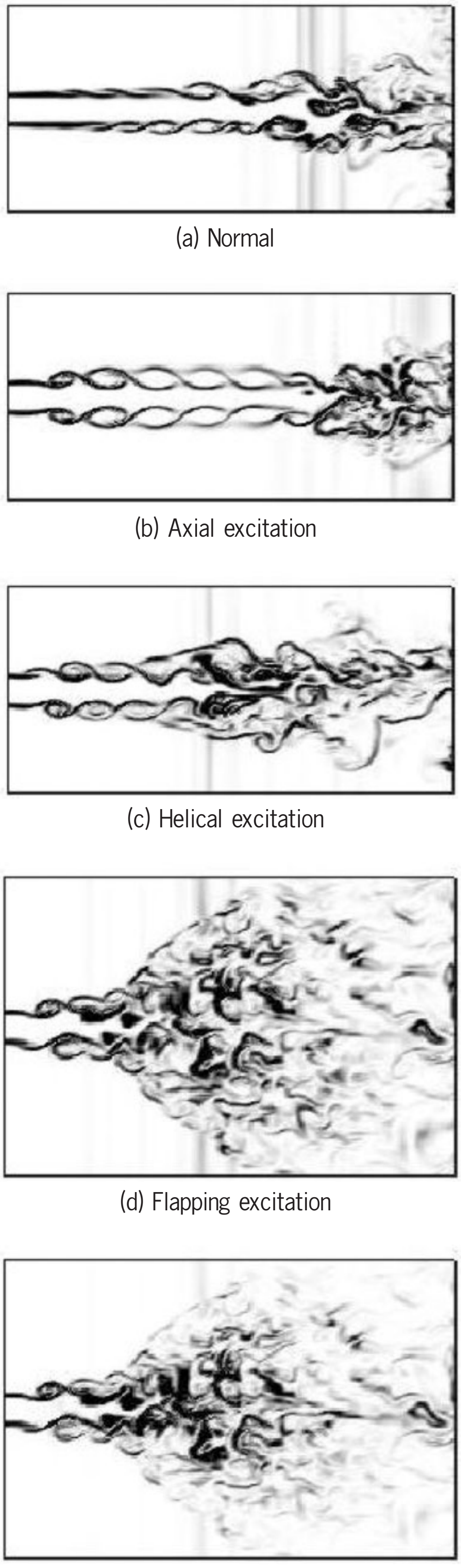

(a) Normal

(b) Axial excitation

(c) Helical excitation

(d) Flapping excitation

(e) Flapping excitation

Figure 9. Contour of production term of the mixing measure on the x–y plane,(a)–(d) for the statistical entropy, (e) for the mixedness parameter.

REFERENCES

[1] Reynolds, W. C., Parekh, D. E., Juvet, P. J. D. and Lee, M. J. D., 2003, Bifurcating and Blooming Jets, *Annu. Rev. Fluid Mech.*, pp.295-315.

[2] Hilgers, A. and Boersma, B. J., 2001, Optimization of turbulent jet mixing, *Fluid Dyn. Res.* **29**, pp.345-368.

[3] Silva, C. B. and Metais, O., 2002, Vortex control of bifurcating jets: A numerical study, *Phys. of Fluids* **14**, pp.3798-3819.

[4] Tsujimoto, K., Shakouchi, T. Sasazaki S and Ando, T., 2006, Direct Numerical Simulation of Jet Mixing Control Using Combined Jets, *JSME Int. J. Ser. B*, **49**-4, pp.966-973.

[5] Everson, R., Manin, D. and Sirovich, L., 1998, Quantification of Mixing and Mixing Rate from Experimental Observations, *AIAA J.* **36**, pp.121-127.

[6] Chikahisa, T., Yuyama, R. and Hishinuma, Y., 2001, A Method for Analyzing Hetrogeneity Degree in Diffusion Process, *Trans. JSME, Ser. B*, **67**-658, pp.1563-1570.

[7] Cetegen, B.M. and N. Mohamad, N., 1993, Experiments on liquid mixing and reaction in a vortex, *J. Fluid Mech.* **249**, pp.391-414.

[8] Tseng, Y. and Ferziger, J., H., 2001, Effects of Coastal Geometry and the Formation of Cyclonic/Anti-Cyclonic Eddies on Turbulent Mixing in Upwelling Simulation, *J. Turbulence* **2** 014, pp.1-23.

[9] Lele, S. K., 1992, Compact finite difference schemes with spectral-like resolution, *J. of Comp. Phys.* **103**, pp.16-42.

[10] Harlow, F. H. and Welch, J. E., 1965, Numerical calculation of time-dependent viscous incompressible flow of fluid with free surface, *Phys. Fluids* **8**, pp.2182-2189.

[11] Hussain, A. K. M. F. and Zaman, K. B. M. Q., 1981, The Preferred Mode of the Axisymmetric Jet, *J. of Fluid Mech.*, **110**, pp. 39-71.

[12] Urbin, G. and Metais O., 1997, Large-eddy simulations of three-dimensional spatially developing round jets, *In Direct and large-eddy simulations* **II**, P.R. Chollet, J.P. Voke and L. Kleiser, Kluwer: Dordrecht, pp. 539-542.